Monthly Notices of the ROYAL ASTRONOMICAL SOCIETY

MNRAS **475,** 788–799 (2018) doi:10.1093/mnras/stx3202
Advance Access publication 2017 December 12

Galaxy And Mass Assembly (GAMA): blue spheroids within 87 Mpc

Smriti Mahajan,[1⋆] Michael J. Drinkwater,[2] S. Driver,[3,4] A. M. Hopkins,[5] Alister W. Graham,[6] S. Brough,[7] Michael J. I. Brown,[8] B. W. Holwerda,[9] Matt S. Owers[5,10] and Kevin A. Pimbblet[11]

[1]*Indian Institute for Science Education and Research Mohali-IISERM, Knowledge City, Manauli 140306, Punjab, India*
[2]*School of Mathematics and Physics, University of Queensland, Brisbane, QLD 4072, Australia*
[3]*International Centre for Radio Astronomy Research (ICRAR), University of Western Australia, Crawley, WA 6009, Australia*
[4]*Scottish Universities' Physics Alliance (SUPA), School of Physics and Astronomy, University of St Andrews, North Haugh, St Andrews KY16 9SS, UK*
[5]*Australian Astronomical Observatory, PO Box 915, North Ryde, NSW 1670, Australia*
[6]*Centre for Astrophysics and Supercomputing, Swinburne University of Technology, Victoria 3122, Australia*
[7]*School of Physics, University of New South Wales, NSW 2052, Australia*
[8]*School of Physics and Astronomy, Monash University, Clayton, VIC 3800, Australia*
[9]*Department of Physics and Astronomy, 102 Natural Science Building, University of Louisville, Louisville, KY 40292, USA*
[10]*Department of Physics and Astronomy, Macquarie University, NSW 2109, Australia*
[11]*E.A. Milne Centre for Astrophysics, University of Hull, Cottingham Road, Kingston-upon-Hull HU6 7RX, UK*

Accepted 2017 December 7. Received 2017 December 6; in original form 2017 October 28

ABSTRACT

In this paper, we test if nearby blue spheroid (BSph) galaxies may become the progenitors of star-forming spiral galaxies or passively evolving elliptical galaxies. Our sample comprises 428 galaxies of various morphologies in the redshift range $0.002 < z < 0.02$ (8–87 Mpc) with panchromatic data from the Galaxy and Mass Assembly survey. We find that BSph galaxies are structurally (mean effective surface brightness, effective radius) very similar to their passively evolving red counterparts. However, their star formation and other properties such as colour, age, and metallicity are more like star-forming spirals than spheroids (ellipticals and lenticulars). We show that BSph galaxies are statistically distinguishable from other spheroids as well as spirals in the multidimensional space mapped by luminosity-weighted age, metallicity, dust mass, and specific star formation rate. We use H I data to reveal that some of the BSphs are (further) developing their discs, hence their blue colours. They may eventually become spiral galaxies – if sufficient gas accretion occurs – or more likely fade into low-mass red galaxies.

Key words: galaxies: evolution – galaxies: fundamental parameters – galaxies: star formation – galaxies: stellar content – galaxies: structure.

1 INTRODUCTION

Traditionally, passively evolving red galaxies have been associated with spheroidal morphology, while optically blue, star-forming galaxies are found to be spiral or irregular. These observations are strengthened by the existence of two distinct loci for red and blue galaxies in the colour–magnitude space: the 'blue cloud' for the star-forming galaxies and the 'red sequence' for the passively evolving spheroids residing in dense environments.

In this paper, we show that this colour–morphology relation breaks down for the blue spheroid (BSph) galaxies,[1] especially below $(g-r)^0 \lesssim 0.5$, or $M*/\mathrm{M}_\odot \lesssim 9$ where spheroidal galaxies are found to be predominantly blue and star forming. Using observed and derived properties of galaxies, in this paper we examine the BSph galaxies as the likely (i) progenitors of passively evolving low-mass elliptical galaxies, (ii) intermediate stage in the evolution of massive spirals, or (iii) unique population different from both the elliptical and spiral galaxies.

Due to their fascinating nature, BSph galaxies have been the subject of many studies in the last few years. Schawinski et al. (2009),

[1] In the context of this paper, BSphs are extremely blue and compact spheroid galaxies. Morphologically, they resemble small elliptical galaxies or bulges of spirals.

⋆ E-mail: mahajan.smriti@gmail.com

for instance, presented a sample of BSphs selected by visual inspection from the Galaxy Zoo. Their sample comprised L^* BSph galaxies at $0.02 < z < 0.05$. They found that BSph galaxies mostly reside in low-density environments, forming ∼6 per cent of all spheroidal galaxies at low redshift. Using the deep Millennium Galaxy Catalogue ($\mu = 26$ mag arcsec^{-2}; Liske et al. 2003), Driver et al. (2006) classified 11.2 per cent of the galaxies at $z \sim 0$ as BSphs, while Cameron et al. (2009) confirmed that BSphs are rare in the local Universe with a volume density of $(1.1 \pm 0.1) \times 10^{-4}\,h_{70}^3\,\mathrm{Mpc}^{-3}$.

Kannappan, Guie & Baker (2009) found that BSph galaxies become more common with decreasing stellar mass, such that their fraction increases from $\lesssim$2 per cent ∼ 1–2 × 10^{11} $M_\odot$ to $\gtrsim$20 per cent below 4–6 × 10^9 $M_\odot$. Since the latter mass scale coincides with the mass scale below which the mean global atomic gas fraction increases for all types of galaxies (Kannappan 2004; Kannappan & Wei 2008; Janowiecki et al. 2017), Kannappan et al. suggested that the presence of cold gas may be crucial to the existence of BSph galaxies. Their findings were complementary to that of Noeske et al. (2006), who analysed a sample of 26 luminous BSph galaxies at high redshift (∼0.2–1.3) to show that most of the BSphs had a smaller, brighter star-forming component with an extended, almost exponential disc-like component with scale length of $\lesssim$ 2 kpc. Based on their results, Noeske et al. (2006) suggested that the majority of BSph galaxies at high-z will evolve into small disc galaxies or low-mass spheroids.[2] They neither find any evidence suggesting inside-out growth scenario which could turn BSphs to large discs, nor do they see any disc growth around BSphs (but see Graham, Dullo & Savorgnan 2015; Graham, Ciambur & Savorgnan 2016; Graham et al. 2017, for an alternative view). Lopes et al. (2016) also investigated a sample of low-z galaxies in various environments. Their analysis suggests that while highly asymmetric BSphs may originate in mergers, the star formation histories of BSphs are likely to be heterogeneous.

In this paper, we utilize the arsenal of data compiled by the Galaxy and Mass Assembly survey (GAMA; Driver et al. 2016), which provides an unprecedented view of low-redshift galaxies using 21-band photometry and fibre-spectroscopic data as discussed in the following section. In Section 3, we analyse the physical properties of BSphs relative to other types of galaxies, and perform automatic classification of all galaxies in multidimensional parameter space in Section 4. We analyse the neutral hydrogen data for our sample, where available in Section 5. We discuss our findings in the context of existing literature in Section 6, and finally summarize our results in Section 7. Throughout this paper, we assume a Λ cold dark matter (ΛCDM) concordance cosmological model with $H_0 = 70\,\mathrm{km\ s^{-1}\,Mpc^{-1}}$, $\Omega_\Lambda = 0.7$, and $\Omega_\mathrm{m} = 0.3$ to calculate all distances and magnitudes.

2 DATA

2.1 Spectroscopic and photometric data

The GAMA survey is a combined spectroscopic and photometric multiwavelength programme. GAMA has measured photometry for over 230 deg^2 on the sky in 21 wavebands, and obtained spectroscopic redshifts for ∼300 000 galaxies ($z \lesssim 0.25$; Baldry et al. 2010; Robotham et al. 2010; Driver et al. 2011, 2016; Hopkins et al. 2013).

The sample used in this paper is the same as that used in Mahajan et al. (2015, hereafter Paper I), but with some of the derived parameters updated in accordance with the latest versions of the GAMA II catalogues (Liske et al. 2015). We direct the reader to Paper I for details of sample selection and its characteristics, highlighting only the most relevant aspects below briefly for completeness. Our sample comprises 428 galaxies[3] selected to have very well-constrained spectroscopic redshifts in the range $0.002 < z_\mathrm{TONRY} < 0.02$.[4] This redshift range was chosen to exclude galactic stars and enable morphological classification of galaxies by visual inspection using shallow (53.9 s band^{-1}) Sloan Digital Sky Survey (SDSS; data release 7) imaging. The spectroscopic campaign for GAMA is based on the SDSS imaging complete to $r < 19.8$ mag, which translates to $M_r = -14.9$ mag at the maximum redshift ($z = 0.02$) of data used in this paper.

We use the matched-aperture photometry measured across 21 wavebands for GAMA galaxies using the Lambda Adaptive Multi-Band Deblending Algorithm in R (LAMBDAR; Wright et al. 2016). Specifically, we use LambdarSDSSgv01, LambdarSDSSrv01, and LambdarInputCatUVOptNIRv01 catalogues from the LAMBDAR data management unit (DMU). The magnitudes are then k-corrected to $z = 0$ using the k-corrections from the kcorr_auto_z00v05 DMU (Loveday et al. 2012). We note that the k-corrections in this DMU have been obtained using the SDSS model magnitudes and GAMA matched aperture AUTO magnitudes from the ApMatchedCatv06 DMU. Since the correlation between the AUTO and LAMBDAR magnitudes for our sample is better than 95 per cent[5], they can be applied to LAMBDAR magnitudes for our sample. The mean k-correction for our sample in the g and r bands is ∼0.009 mag.

2.2 Physical properties of galaxies

The best-fitting values for several physical parameters for all galaxies in the three equatorial regions of the GAMA survey have been obtained by running the spectral energy distribution fitting code Multiwavelength Analysis of Galaxy Physical Properties (MAGPHYS; da Cunha, Charlot & Elbaz 2008) on the 21-band photometry taken from the Lambdarcatv01 DMU (Driver et al. 2016). We use the stellar mass (M^*), star formation rate (SFR), r-band light-weighted age, and metallicity (Z) obtained from the MAGPHYS DMU (version 6) in our analysis below.

The SFR derived from MAGPHYS is an integrated measure of the SFR and therefore represents the star formation activity of a galaxy averaged over a long period of time (0.1 Gyr for MAGPHYS). It may thus be argued that for galaxies undergoing a strong burst of star formation, MAGPHYS-derived SFR may be very different from the instantaneous SFR. In order to test this hypothesis, we converted the Hα equivalent width (EW)[6] to luminosity using equation 5 of Hopkins et al. (2003).[7] The instantaneous (<10 Myr) SFR is then estimated using the luminosity-to-SFR conversion factor given by Kennicutt (1998).

Fig. 1 shows a comparison between the two measures of SFR for our sample. On average, the MAGPHYS-derived SFR is ∼0.6 dex

[2] Throughout this paper, we collectively refer to lenticulars, BSphs, and elliptical galaxies as spheroids unless stated otherwise.

[3] All but four galaxies from Paper I are excluded because of missing data in GAMA II catalogues.

[4] z_TONRY uses the flow model described in Tonry et al. (2000).

[5] >98 per cent excluding irregular galaxies from our sample.

[6] The EW (Hα) is obtained from the SpecLineSFRv05 (Gordon et al. 2017).

[7] We assume a constant stellar absorption correction of 2.5 Å as in Gunawardhana et al. (2013).

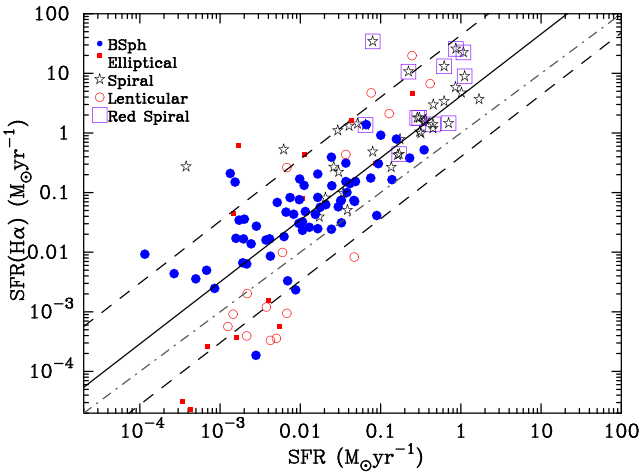

Figure 1. Comparison between MAGPHYS-derived 'average' SFR and the instantaneous SFR measured from the Hα emission line. The solid and the dashed *black* lines represent the linear least square fit and $\pm1\sigma$ deviation therein to the 415 galaxies for which data are available. The *grey* dot–dashed line represents equal SFR on both axes. For our sample, a constant offset can be applied to the MAGPHYS-derived SFR to get instantaneous SFR.

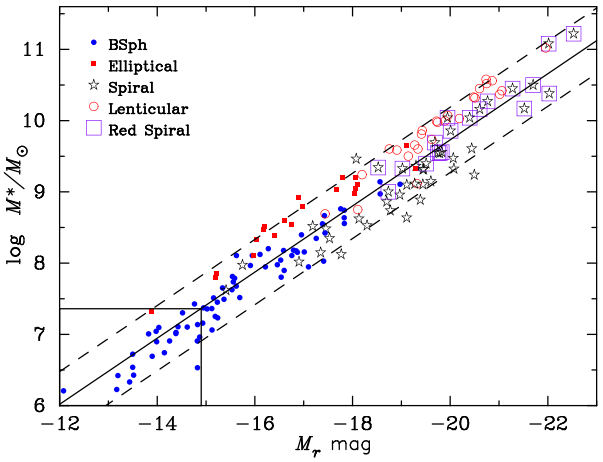

Figure 2. Stellar mass (log$M^*/M_\odot$) as a function of r-band absolute magnitude for our sample. The rectangular region at the bottom left marks the zone of incompleteness in this space.

lower than the H α SFR. We therefore conclude that for the sample used here, the average SFR can be converted to an instantaneous SFR by using a simple scaling factor. The use of the latter instead of former will only change our results qualitatively. We therefore use the MAGPHYS-derived 'average' SFR throughout.

Fig. 2 shows that the absolute r-band magnitude and MAGPHYS-derived M^* for our sample are well correlated[8] as $\log M^*/M_\odot = 0.450–0.464\,M_r \pm 0.458$. Based on this figure and the limiting magnitude of $M_r = -14.9$ mag, in the following we adopt $\log M^*/M_\odot = 7.36$ as the limiting stellar mass for our sample. 16.3 per cent (27/165) of the galaxies shown in Fig. 2 fall in the incomplete zone (the fraction increases to ∼30 per cent when Irr and LSB galaxies are included). For completeness, we show all data points in the following figures, highlighting the ones in the incomplete zone of the M^*–M_r space.

2.3 Morphological classification

The morphological classification of galaxies used in this work is the same as that in Paper I and we direct the reader to section 3.1 therein for details, briefly summarizing our methodology below for completeness. Visual classification of the three-colour *giH* images[9] of all galaxies in the redshift range 0.002–0.02 was done by Mahajan, Driver, and Drinkwater multiple times. Some representative examples of the postage stamp images classified into different categories are shown in Fig. 3. We found that in the chosen redshift range, our data could be categorized into six classes:

(i) *Elliptical:* Galaxies which are morphologically elliptical in shape. They are mostly red in colour.

(ii) *Spirals:* Galaxies showing well-defined spiral arms or clearly identifiable edge-on discs. These galaxies often show conspicuous signs of ongoing star formation, such as H II regions, and stellar associations forming spiral arms.

(iii) *Lenticulars:* Red, disc galaxies with a resolved nucleus. These galaxies are mostly big and bright, occasionally showing signs of some ongoing star formation in rings around nucleus, or low surface brightness discs without spiral arms.

(iv) *BSphs:* Colour plays a key role in successfully identifying these galaxies. They are very blue and generally compact spheroids, morphologically similar to small elliptical galaxies or bulges of spiral galaxies.

(v) *Low surface brightness (LSB) galaxies:* These extended objects show very poor contrast with the background in the five-band SDSS imaging. We note that a substantial fraction of these galaxies may have been misclassified due to the very shallow imaging data used here. Many of these galaxies may also be classified as irregular, and as we will show below, these two classes overlap in most of the parameter space explored here.

(vi) *Irregulars (Irr):* All confirmed extended sources that do not belong to any of the above categories.

Although we did not use luminosity in our classification scheme, the results were luminosity-dependent, such that the latter three classes (BSphs, LSBs, and Irr) dominate the low-luminosity regime in our sample, with irregulars being the most dominant population (∼45 per cent), followed by BSphs (∼17 per cent).

415/428 (97 per cent) of our sources are also found in the VisualMorphologyv03 DMU of GAMA. In our chosen redshift range, we find 57 (14 per cent) galaxies are classified as the 'little BSphs' in the VisualMorphologyv03 DMU, of which 29 (40 per cent) are also classified as BSphs in this paper.

Table 1 gives the GAMA II IDs, r-band magnitude, and the uncertainty in it, and redshifts compiled from the above mentioned DMUs along with the morphological classification (as per Paper I) for all the galaxies in our sample. The morphological classification is 1: Elliptical, 2: Spiral, 3: Irregular, 5: BSph, 6: LSB, and 11: Lenticular. Since the focus of this paper is to compare BSphs with spirals and other spheroids, in the following we only show the 165 galaxies which are identified into one of these morphology classes unless specified otherwise. A complete version of Table 1 is

[8] Although not shown for clarity, all 428 galaxies were included in evaluating the least square fit relation and the scatter therein.

[9] Each image is generated using the SDSS g, i and the UK Infrared Telescope (UKIRT) Infrared Deep Sky Survey (UKIDSS) Large Area Survey (LAS) H-band data (http://www.ukidss.org/surveys/las/las.html).

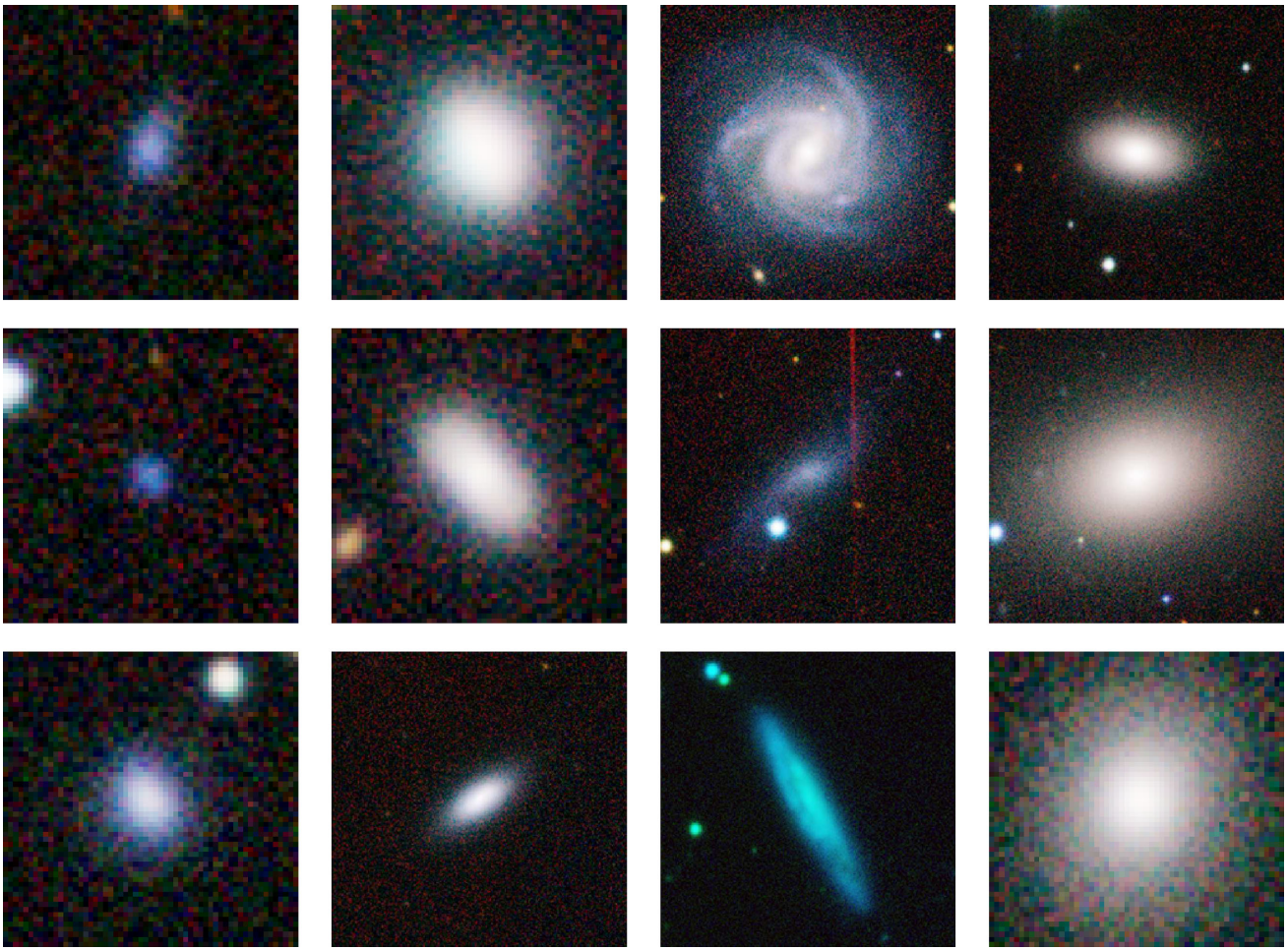

Figure 3. Some examples of different morphological types of galaxies. Images are grouped along columns (from left): (i) BSphs, (ii) Ellipticals, (iii) Spirals, and (iv) Lenticulars. Each *giH* image is scaled to a constant physical size of 20 × 20 square kpc at the redshift of the galaxy.

Table 1. Complete sample of 428 galaxies (a complete version of this table is available online). The morphology classification (column 4) is: 1: Elliptical, 2: Spiral, 3: Irregular, 5: BSph, 6: LSB, and 11: Lenticular.

GAMA ID	M_r mag	ΔM_r mag	Morphology	z	ALFALFA ID	H I Flux (S_i) Jy km s^{-1}	ΔS_i Jy km s^{-1}	log H I $M_\odot$
105589	19.67	0.03	3	0.019	–	–	–	–
106916	19.58	0.04	6	0.015	249428	0.63	0.05	8.72
107137	13.94	0.01	11	0.015	–	–	–	–
107226	19.39	0.03	6	0.016	–	–	–	–
116572	19.84	0.02	6	0.020	–	–	–	–
117059	19.87	0.04	5	0.011	–	–	–	–
118764	18.47	0.09	3	0.011	–	–	–	–
119004	17.87	0.05	3	0.013	–	–	–	–

available online. Any further information for any of the 428 galaxies from this sample can be obtained from the GAMA website[10] by using the unique GAMA IDs.

3 ANALYSIS OF PHYSICAL PROPERTIES

In this section, we discuss the trends in various physical properties for the galaxies in our sample, briefly discussing how each of them may contribute towards our understanding of the evolution of the BSph galaxies.

3.1 Luminosity and colour

In Fig. 4, we show the distribution of spheroidal and spiral galaxies in the colour–magnitude diagram. While the BSphs occupy the region with the bluest colours irrespective of the magnitude, the lenticulars are the most luminous and optically red in colour. The elliptical galaxies have red colour similar to lenticulars, but are less luminous than the latter. Almost 2/3rd of the spiral galaxies have

[10] http://www.gama-survey.org/

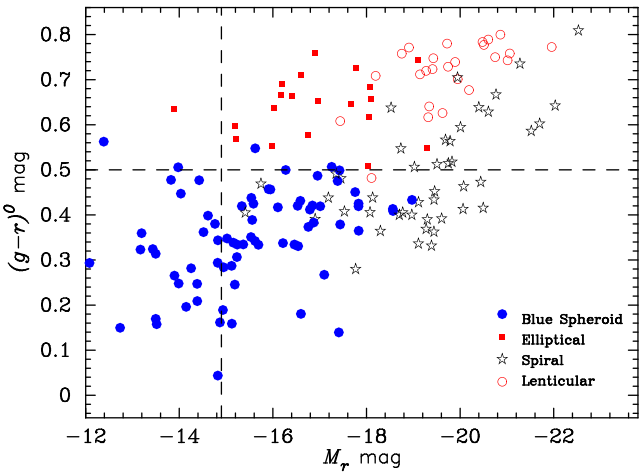

Figure 4. The spiral and spheroidal galaxies (Lenticulars, Ellipticals, and BSphs) in the colour–magnitude space. The horizontal dashed line is the colour-cut used for separating blue and red spiral galaxies at $(g-r)^0 = 0.5$ mag, and the vertical dashed line is the r-band completeness limit corresponding to $z_{max} = 0.02$.

$(g-r)^0 \sim 0.4 \pm 0.1$ mag, but the rest of them acquire increasingly redder colour as they become more luminous than $M_r \sim -18.5$ mag. Fig. 4 as well as visual inspection of spiral galaxies in our sample suggests that $(g-r)^0 = 0.5$ mag is a good divider for segregating blue spirals from red ones. The red spirals are marked in all the following figures to distinguish them from their blue counterparts.

Fig. 4 shows that the passively evolving galaxies (ellipticals and lenticulars) and star-forming spirals and BSphs form a continuous distribution in the optical colour–magnitude space.

3.2 Star formation

In Fig. 5, we show the distribution of the SFR and SFR/M^* for galaxies with different morphologies as a function of their r-band absolute magnitude. The BSphs and spirals form a sequence such that the SFR increases with luminosity, according to the fitted relation represented by a solid line in the top panel of Fig. 5. The passively evolving ellipticals and lenticular galaxies also seem to follow a similar relation although with a lower normalization factor. This trend is replicated for the SFR/M^*, although with a lower slope for the fitted relation since most of the star-forming galaxies (BSphs and spirals) have SFR/M^* in the range 10^{-8}–10^{-10} yr^{-1}, unlike their log SFR which varies by ∼5 dex. The log SFR/M^* for the passively evolving ellipticals and lenticulars on average decreases by >2 dex relative to the star-forming galaxies. The r-band absolute magnitude is related to the SFR and SFR/M^* in Fig. 5 by the relations:

$$\log \mathrm{SFR}(\mathrm{M}_\odot\ \mathrm{yr}^{-1}) = -0.381\, M_r - 8.029 \pm 0.486 \quad (1)$$

and

$$\log \mathrm{SFR}/M^*(yr^{-1}) = 0.084\, M_r - 8.367 \pm 0.605, \quad (2)$$

where the uncertainty is the 1σ deviation in the fitted linear least squares relation for star-forming galaxies (BSphs and spirals only).

These trends in the SFR and SFR/M^* show that BSph galaxies are closer to spirals than ellipticals in the sense that they follow the same relation as the spirals, mostly occupying the lower (higher) edge of the SFR (SFR/M^*) distribution.

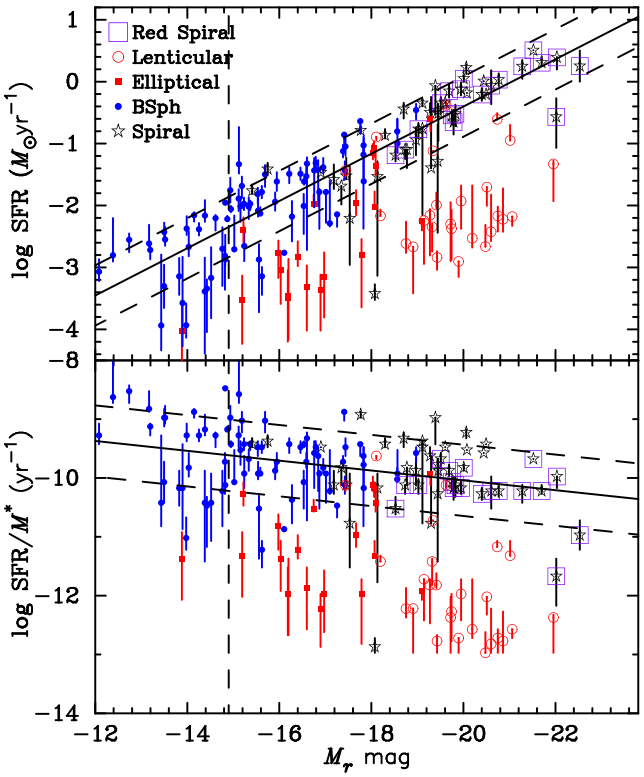

Figure 5. The SFR (top) and SFR/M^* (bottom) for our sample of galaxies as a function of M_r. Symbols and vertical line are same as in Fig. 4. The solid line is the linear least square fit to the BSphs and spiral galaxies, while the dashed lines represent 1σ deviation in the fitted relation.

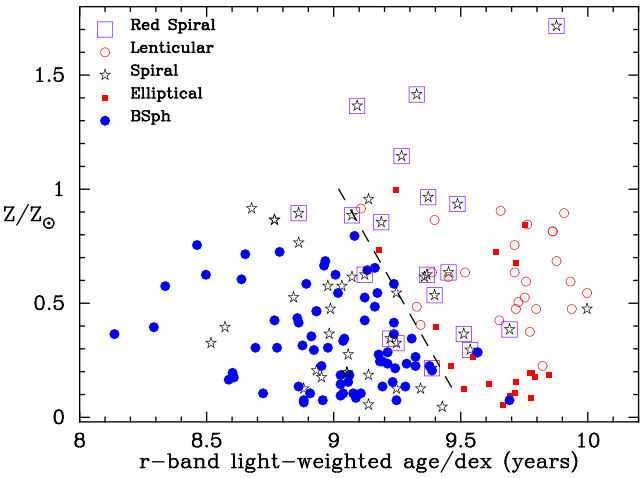

Figure 6. Galaxies in the age–metallicity plane. The purple open squares around stars represent red spiral galaxies identified in Fig. 4. The dashed line is shown to guide the eye to the division between star-forming and passive galaxies in this space.

3.3 Age and metallicity

In Fig. 6, we show the distribution of our galaxies in the age–metallicity space. The star-forming spirals and BSphs cluster together in the left of the diagram at lower age and metallicity (Z), while the ellipticals coincide with the lenticulars in the other half. As expected, most of the red spirals identified in Fig. 4 are found

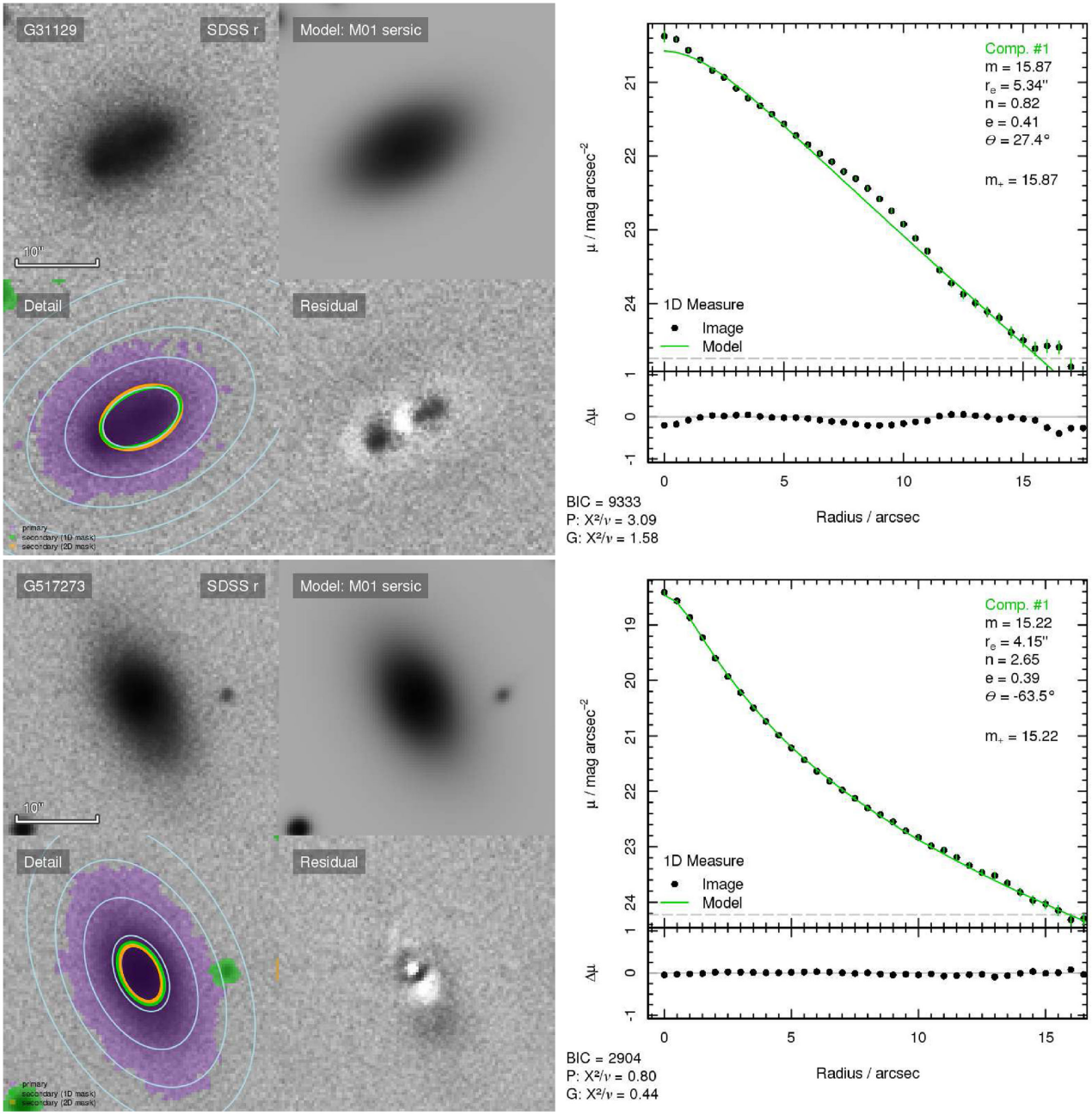

Figure 7. The surface brightness fits in the SDSS *r* band for two BSph galaxies. Each panel shows (clockwise from top left:) the original SDSS *r*-band image, Sérsic model, 1D light profile (with residuals: image-model at the bottom), residual image, and ellipses centred on the primary galaxy used for estimating the light profile along with masked objects, respectively.

closer to the dividing line, or coincide with the passively evolving galaxies in this age–metallicity space. At least half of the red spirals on average also have greater *Z* than the lenticulars. We show an approximate dividing line in Fig. 6 to guide the eye to the suggested division between the star-forming and passively evolving galaxies. The significance of this line will become clear in the next section where we employ an automated algorithm to find clusters of galaxies based on various combinations of other physical properties.

Since BSph galaxies coincide with star-forming spirals in Fig. 6, it can be concluded that they may have shared similar star formation histories.

3.4 Structural properties

Light profiles of all galaxies in the GAMA data base in 20 wavebands were fitted using a single Sérsic profile using the Structural Investigation of Galaxies via Model Analysis (SIGMA, v1.0-2; Kelvin et al. 2012). The properties of our sample as outputted by SIGMAare described in Paper I. Figs 7 and 8 show two examples each of BSph galaxies and ellipticals in SDSS *r* band. The residual images evidently show the presence of a disc or a nuclear component in addition to the bulge modelled by the single-Sérsic profile in these systems. Such non-negligible residuals are found for ∼43 per cent of ellipticals and ∼38 per cent of BSph galaxies in our sample. This is consistent with the fraction (∼42 per cent) found

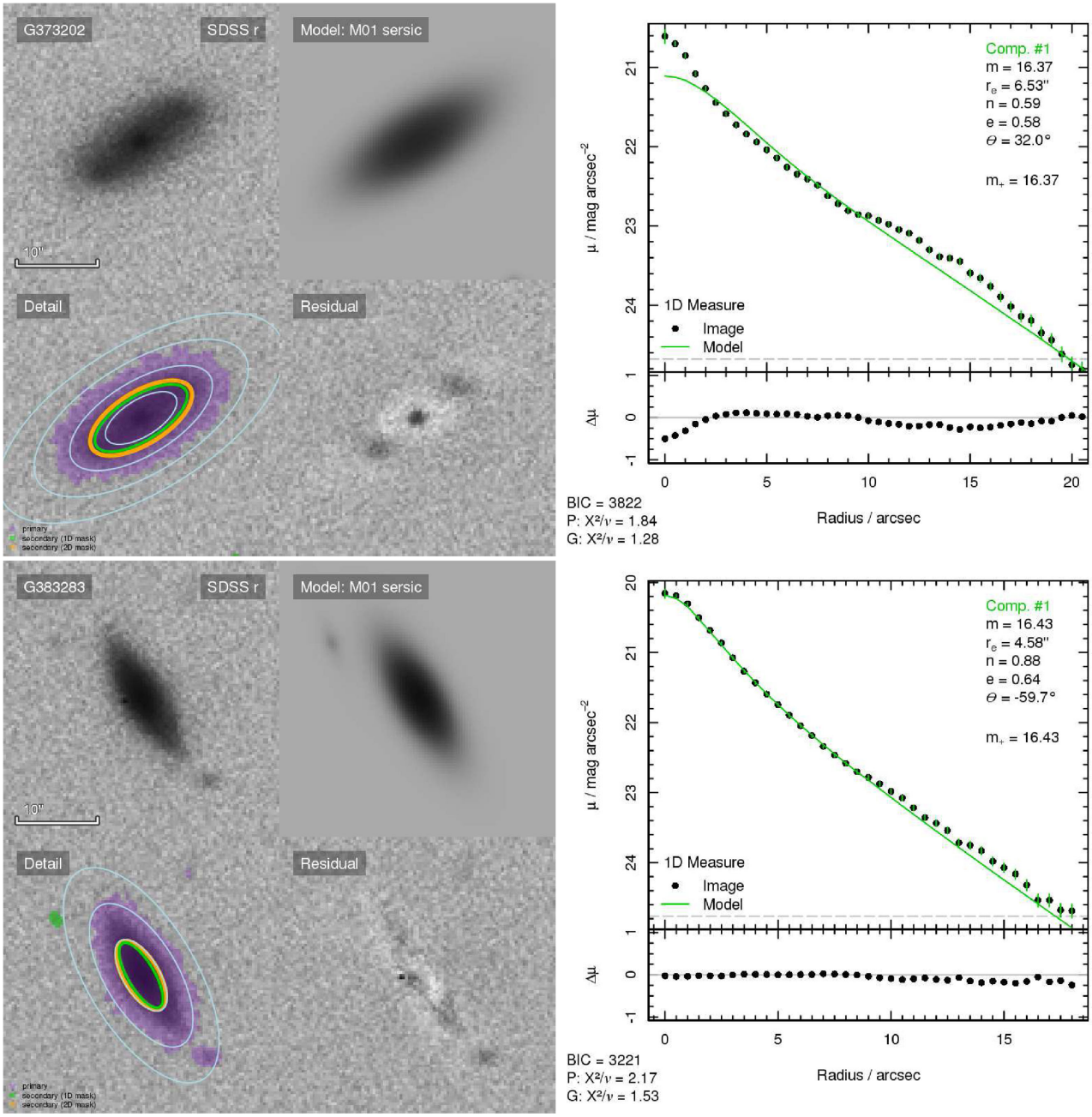

Figure 8. Same as Fig. 7, but for elliptical galaxies.

by George (2017). Together these results elucidate that although this class of galaxies is termed BSphs here (and 'little BSphs' or 'blue ellipticals' or 'blue early-type galaxies' elsewhere), structurally they can be further subdivided into at least two different types: genuine BSphs, and blue dwarf elliptical galaxies which can be resolved into two components, and therefore should instead be called blue dwarf 'lenticulars' instead of ellipticals or spheroids.

In Fig. 9, we show the 2D space mapped by the structural parameters $R_{\rm eff}$ and average surface brightness ($\langle\mu\rangle_e$) as a function of M_r and M^* and the latter two with each other. Fig. 9 reiterates our results from Paper I, i.e. BSph galaxies are structurally similar to ellipticals, spanning the same range of $R_{\rm eff}$, $\langle\mu\rangle_e$, luminosity, and M^*. Fig. 9 (c) shows that BSphs, ellipticals, and red spirals form a single sequence in the stellar mass-$R_{\rm eff}$ space, but star-forming spirals and lenticulars deviate away from the mean sequence such that at any M^* on average star-forming spirals are larger and lenticulars are smaller than the red spirals. Fig. 9 (d) shows that all spheroids follow the same mean relation of declining $\langle\mu\rangle_e$ with increasing luminosity. But at fixed luminosity, spirals always have higher surface brightness relative to the spheroids.

In a nutshell, this section shows that BSph galaxies are structurally similar to their passively evolving counterparts, but resemble star-forming spirals in age, Z, and star formation properties. In the following section, we examine the clustering properties of galaxies using automatic clustering algorithm and reanalyse their distribution in some of the parameter spaces discussed above.

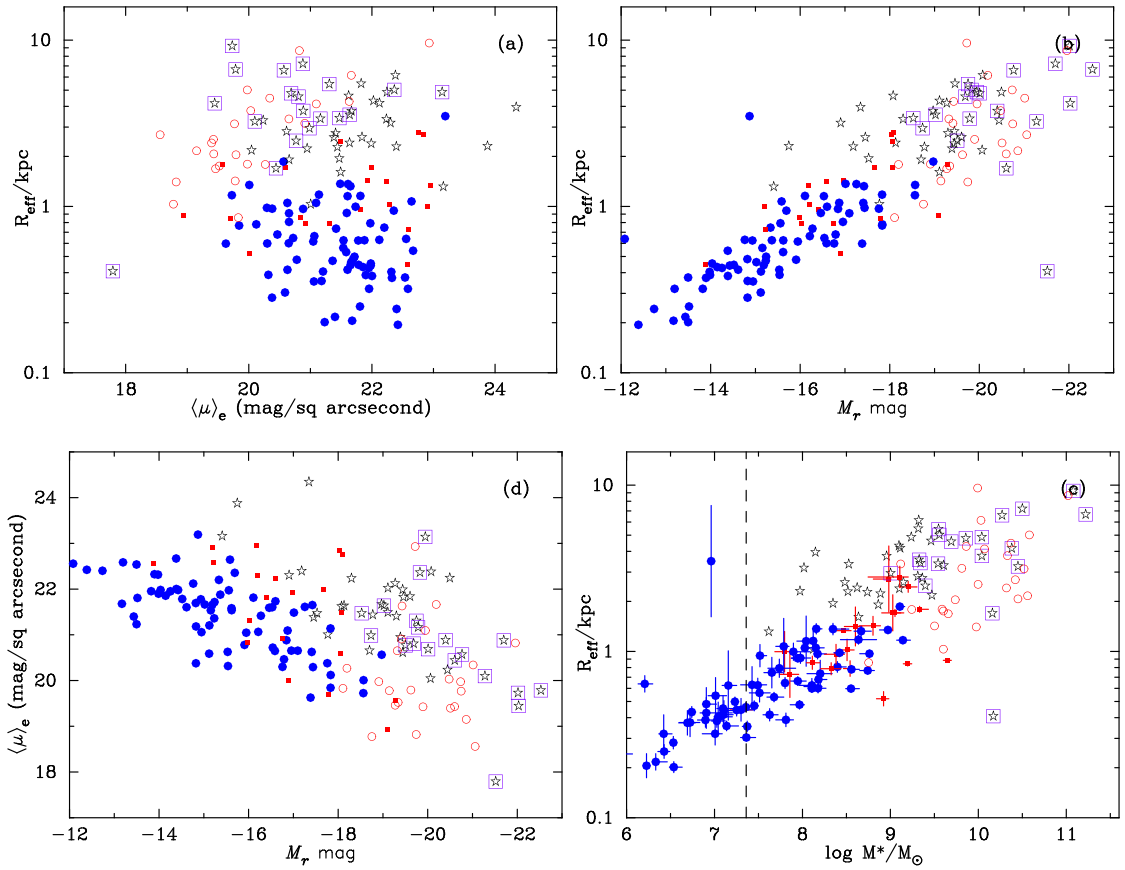

Figure 9. Scaling relations for bulge-dominated and spiral galaxies. Effective radius ($R_{\rm eff}$) is shown as a function of (a) average surface brightness, (b) absolute r-band magnitude, and (c) stellar mass. Panel (d) shows the average surface brightness as a function of M_r.

4 K-MEANS CLUSTERING ANALYSIS

One approach to test for connections between different galaxy populations is to examine the clustering properties of their parameters. Specifically, we used an objective clustering algorithm to test if the blue spheroidal galaxies were assigned to a group of their own, or if they clustered with either the spiral or the elliptical galaxies in our sample. We used the 'k-means' algorithm (MacQueen 1967) to decompose the data into a specified number of clusters. For a given number of clusters, this finds the cluster positions that minimize the sum of the squares of the distances from each data point to its cluster centre. We determined the best number of clusters to adopt by using the NBCLUST (Charrad et al. 2012) package in the R programming language. This package uses 23 different methods for determining the best number of clusters and selects the number proposed by the most methods. Before starting the clustering analysis, we removed any objects with missing data and then scaled the remaining galaxies to have a mean of zero and a standard deviation of unity in each parameter. All the parameters we analysed were logarithmic measurements (or magnitudes). This approach is very similar to our analysis in Paper 1.

We applied the clustering analysis to several combinations of MAGPHYS parameters reflecting the stellar populations: age, metallicity, stellar mass, dust mass, and specific star formation rate (sSFR). These are listed in Table 2.

For the first analysis, we considered age, metallicity, and M^*. In this case, two clusters were preferred, containing 88 and 77 galaxies, respectively (see Table 2). The larger cluster has galaxies at lower ages, metallicities, stellar masses, and dust masses, as shown in Figs 10 (a), (b), and (c). This cluster contains 92 per cent of the BSphs, but is strongly (24 per cent) contaminated by other galaxy types. The smaller cluster contains 67 per cent of the spiral galaxies and 87 per cent of the passive (elliptical and lenticular) galaxies. This partition has therefore demonstrated some separation between the BSphs and both the other main galaxy types.

For the second analysis, we replaced stellar mass with specific star formation. In this case also two clusters were preferred (see Table 2). The largest cluster again contained galaxies at lower ages, metallicities, dust masses, and stellar masses. This cluster contains 97 per cent of the BSphs, but is heavily (41 per cent) contaminated by other galaxy types than for the first analysis.

For the third analysis, we added in dust mass. In this case, three clusters were preferred, as shown in Figs 11 (a), (b), and (c) (see Table 2). The largest cluster comprising BSphs contained 74 galaxies and 85 per cent of all BSphs in our sample, but is comparatively less contaminated (16 per cent) by other galaxy types. We further note that adding in stellar mass to this list (analysis 4) reduces the contamination by other galaxy types, by effectively removing some of the spirals from the cluster containing BSphs, but does not increase the completeness fraction of BSphs in their cluster.

In summary therefore, the clustering analyses we applied have separated the BSphs from both the spiral and the passively evolving spheroids in our sample. This also evidently shows that once all the four parameters namely, age, Z, SFR/M^*, and $M_{\rm dust}$ are taken into account, BSphs are statistically different from both spirals and ellipticals.

Table 2. Automated classification results.

Analysis	Parameters	N_g	N_c	n_1	n_2	n_3	p_{bsph}	p_{other}
1	Age, Z, M_*	165	2	88	77	–	92 per cent	24 per cent
2	Age, Z, SFR/M^*	165	2	120	45	–	97 per cent	41 per cent
3	Age, Z, SFR/M^*, M_{dust}	165	3	74	50	41	85 per cent	16 per cent
4	Age, Z, SFR/M^*, M_{dust}, M_*	165	3	69	59	37	84 per cent	12 per cent

Notes. N_g is the number of galaxies in the sample, N_c is the preferred number of clusters, and n_i are the number of galaxies assigned to cluster i. p_{bsph} is the percentage of all visually classified BSph galaxies assigned to the first cluster and p_{other} is the percentage of all galaxies in the first cluster which were not classified as BSph.

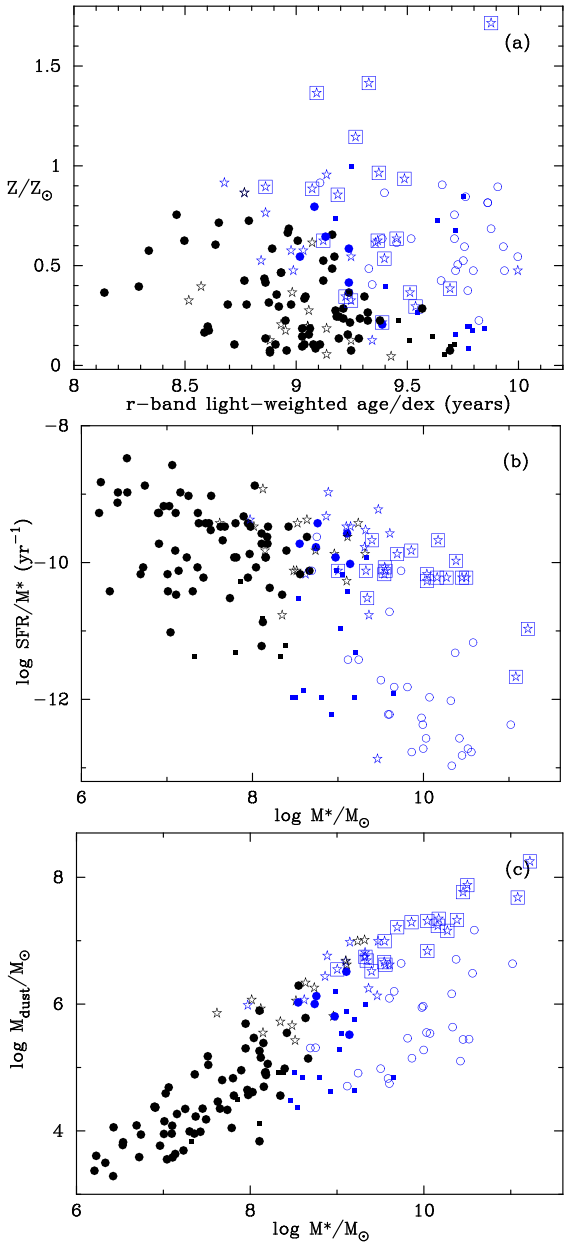

Figure 10. Automated classification of galaxies in our sample. Panel (a) is the same as Fig. 6, but colour-coded for 'clusters' identified by the k-means algorithm using age, Z, and SFR/M^*. The other two panels show the distribution of (b) sSFR, and (c) M_{dust} as a function of M^* for the galaxies belonging to the two clusters preferred by k-means. The symbol types are same as in the above figures. Two clusters are preferred statistically for this set of parameters. The BSphs are statistically well separated from the spirals as well as the ellipticals.

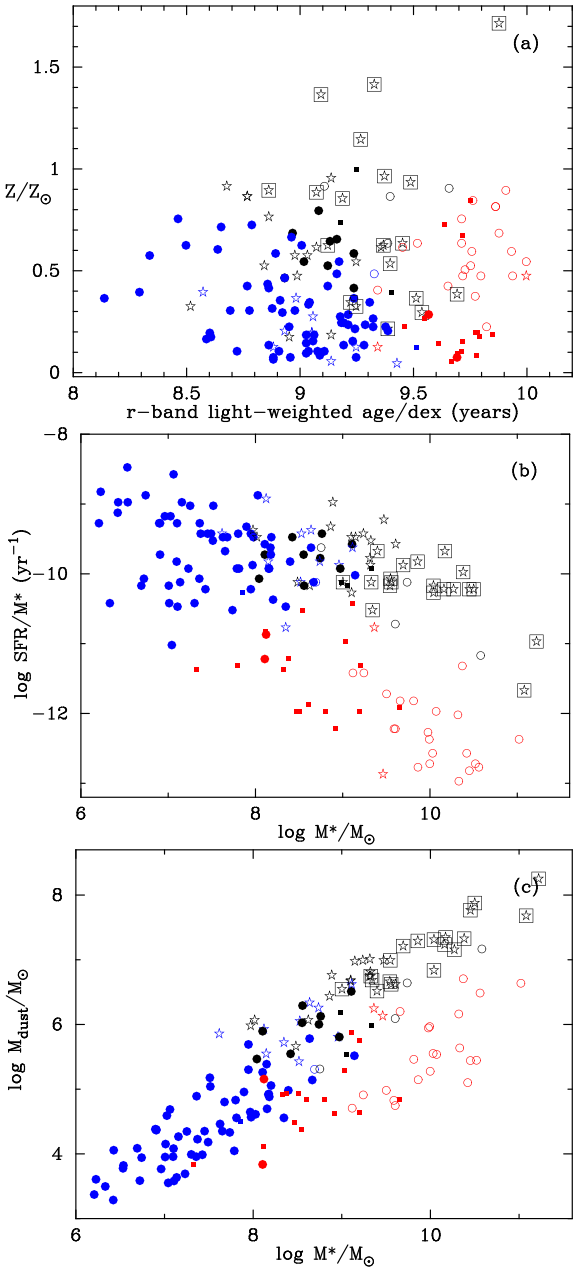

Figure 11. Same as Fig. 10 but for parameters age, Z, SFR/M^*, and M_{dust}. In this case, three clusters are preferred by k-means. The BSphs are statistically well separated from the spirals as well as the ellipticals.

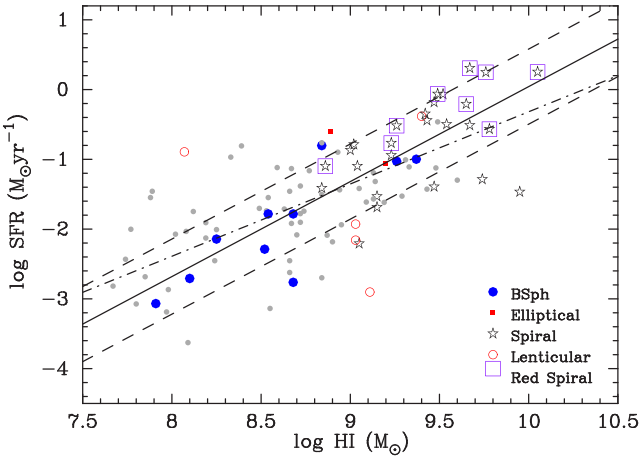

Figure 12. SFR as a function of the atomic gas mass for the galaxies in our sample for which H I data are available. The coloured symbols are the same as in Fig. 2, while the grey points represent irregular and LSB galaxies. The solid and dashed lines are the linear least squares fit and $\pm 1\sigma$ deviation in it, respectively, considering 10 BSphs and 26 spiral galaxies only. The dot–dashed line represents the least squares fit line for all the 101 galaxies detected in H I by the ALFALFA survey.

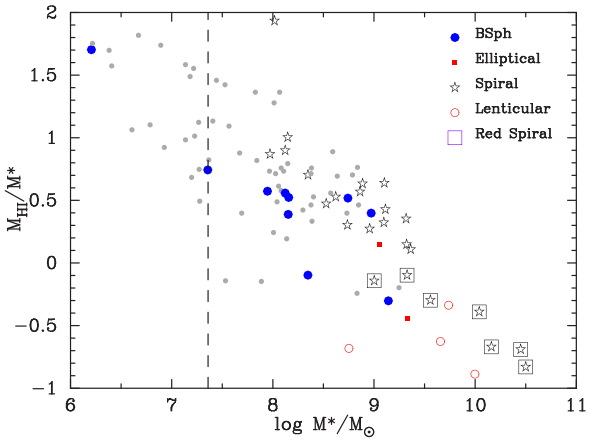

Figure 13. This figure shows the ratio of H I and stellar mass of galaxies detected by the ALFALFA as a function of their stellar mass. The dashed line is the limiting stellar mass for our sample as per Fig. 2.

5 ATOMIC GAS MASS

Recent and current evolution of star formation properties of galaxies is strongly dependent on the amount of gas contained in them. Similarities in the star formation properties of BSph galaxies and spirals suggest that they may obey similar SFR–$M_{\rm gas}$ scaling relation. In order to test this hypothesis, we make use of the Arecibo Legacy Fast ALFA survey (ALFALFA; Giovanelli et al. 2005) which is a blind extragalactic H I survey done using the Arecibo telescope to conduct a census of the local H I universe over a cosmologically significant volume.

101/428 galaxies in our sample have been detected by the ALFALFA survey with a median(mean) signal-to-noise ratio (SNR) of 12(25), and SNR $\geq$ 4.6. To find the H I counterparts, we matched the LAMBDAR position coordinates to the coordinates of the optical counterpart found by the ALFALFA team (Haynes et al. 2011). All except seven of the 101 sources from our sample are matched to counterparts within 5 arcsec (maximum separation 9 arcsec) from the optical counterpart of the H I source as described above; five of these are irregular galaxies, and one each is an LSB and a spiral galaxy, respectively. These seven sources are included in Figs 12 and 13.

In Fig. 12, we show the SFR of different morphological types of galaxies as a function of their H I mass. For completeness, we show all the 101 galaxies from our sample detected by the ALFALFA survey. For all galaxies, SFR is positively correlated with H I mass with a slope of 1.36 $\pm$ 0.54. The red spirals lie above the mean relation, suggesting that these galaxies have higher SFR than expected for their H I mass. The BSphs seem to follow the mean scaling relation as all the other star-forming galaxies in this space. These observations suggest that even if a BSph develops a disc and moves rightward towards higher M^* and SFR in Fig. 12, it is likely to obey the same scaling relation as the spirals, only a few of which significantly deviate away from it. But since only two ellipticals are detected in H I, these observations are inconclusive about the fate of the BSphs once the star formation and gas supply fade away.

6 DISCUSSION

The aim of this paper is to test whether BSph galaxies could be progenitors of spirals or passively evolving elliptical galaxies or if they form a different class of their own based on their structural, physical, and star formation properties. BSph galaxies form around 20 per cent of all low-mass ($M*/M_\odot < 10^9$) galaxies, and 82.5 per cent of all low-mass spheroids in our sample, which is in agreement with the fractions found by Kannappan, Guie & Baker (2009). Furthermore, Moffett et al. (2016) found that the 'little BSphs' classified in the GAMA visual morphology DMU contribute $\sim$2 per cent of the stellar mass density at $0.002 < z < 0.06$. Our analysis showed that BSphs are structurally very similar to low-mass elliptical galaxies. The fraction of elliptical and BSph galaxies which are likely to contain a disc or other components missed by a single Sérsic profile used for fitting the galaxies is also similar (Figs 7 and 8; also see George 2017).

The deep imaging data from the SDSS Stripe 82 have been examined to look for tidal features in the red sequence elliptical galaxies and BSphs. While Kaviraj (2010) found that only 28$\pm$3 per cent of the 238 ellipticals in their sample show tidal features, George (2017) found a fraction of 58$\pm$7 per cent for the BSphs using analysis of residual images similar to the ones shown in Fig. 7. George (2017) also found that tidal features are more common around massive BSphs ($M*/M_\odot > 10^{10.5}$), which are absent in our sample. But since the detection of such features depends upon the depth of the imaging data (see for instance table 3 of Kim et al. 2012), it is not surprising that we fail to find any significant differences between the residual images of ellipticals and BSphs using the shallow SDSS r-band imaging data.

The scaling relations (Fig. 9) for spheroids and spirals show that BSphs occupy similar range of parameters: $R_{\rm eff}$, $M*$, and $\langle\mu\rangle_e$ as the red ellipticals. This implies that if BSphs are ellipticals experiencing strong starburst, the phenomenon causing starburst has left their morphology unchanged. The 10 BSphs from our sample which were detected by the ALFALFA survey show a significant amount of atomic gas. Fig. 13 shows that the median (and mean) ratio of atomic gas to stellar mass in BSphs is $\sim$0.5. It also shows that even in this small sample of BSphs, the ratio $M_{\rm H\,I}/M^*$ varies by $\sim$2 dex over an $M*$ range of two orders of magnitude, suggesting that the evolution history of BSphs is very heterogeneous.

Following Kannappan, Guie & Baker (2009), we estimated the stellar mass doubling time as the stellar mass divided by the SFR,

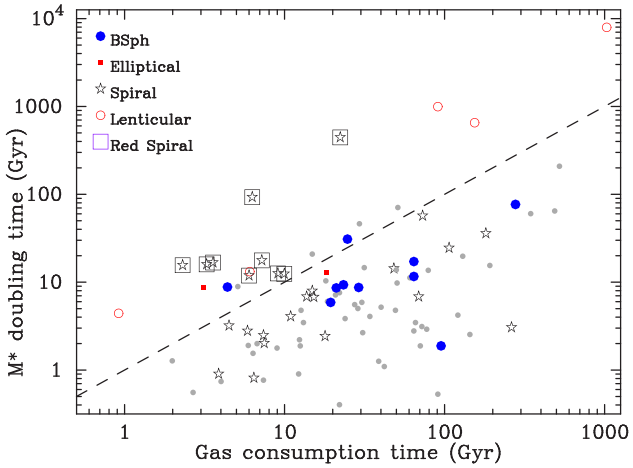

Figure 14. The stellar mass doubling time as a function of the gas depletion time-scale for the ALFALFA detected galaxies in our sample. The dashed line represents the path followed by galaxies which have enough gas to double their stellar mass by continuing to form stars at the present rate. Symbols are same as in Fig. 12.

and gas depletion time-scale as the atomic gas mass divided by the SFR. These time-scales are crude approximations uncorrected for future infall of new gas or decline of star formation. Fig. 14 shows these two time-scales for the galaxies in our sample for which H I data are available. Assuming that the unmeasured molecular gas mass in these galaxies is not very large, galaxies on the left of the line of equality cannot double their stellar mass without accreting new gas. Fig. 14 therefore shows that most BSph galaxies (8/10) can evolve significantly even under the hypothetical closed-box scenario assumed here, and hence may not undergo any morphological changes.

But if a BSph needs to develop a disc similar to a spiral galaxy, its radius must increase by a factor of ∼3 (Fig. 9), implying a large increase in mass. So along with the presence of large amount of gas, BSphs should form stars with great efficiency. The gas consumption time-scale shown in Fig. 14 crudely represents the inverse of star formation efficiency, i.e. $SFE = SFR/M_{\rm HI}$. Even in our small sample, it is evident that the BSphs are on average less efficient at forming stars than spiral galaxies. It is therefore plausible but not mandatory that at least some of the BSph galaxies may evolve into small disc galaxies (also see Noeske et al. 2006).

Using nearby ($z \sim 0.1$) galaxies more massive than a few times $10^9\,{\rm M}_\odot$ from the SDSS, Kauffmann et al. (2006) reported a critical stellar surface mass density, $\log\,\mu_* \sim 3 \times 10^8\,{\rm M}_\odot\,{\rm kpc}^{-2}$ above which the star formation in disc-dominated galaxies occurs in short-lived intense bursts. We estimated $\mu_* = M^*/\pi R^2_{\rm eff}$ for all the galaxies in our sample. Fig. 15 shows μ_* for the spheroids and spiral galaxies[11] as a function of their $M*$, SFR, and sSFR, respectively. For our sample, only 28 galaxies have μ_* greater than the critical threshold, of which 17 (61 per cent) are passively evolving lenticulars and six (21 per cent) are red spirals.

Fig. 15 shows that the stellar surface mass density is strongly correlated with stellar mass irrespective of galaxy morphology. The SFR is found to be a function of μ_* for the BSphs and spirals, but not for the ellipticals and lenticulars. The sSFR for BSph and

[11] Two BSphs and one red spiral galaxy at $\mu_* = 5.37$, 6.09, and 10.45 ${\rm M}_\odot\,{\rm kpc}^{-2}$ do not appear in the figure because of the chosen range for the ordinate. Both the BSphs fall below the mass completeness limit; log $M* = 10.17\,{\rm M}_\odot$ for the red spiral.

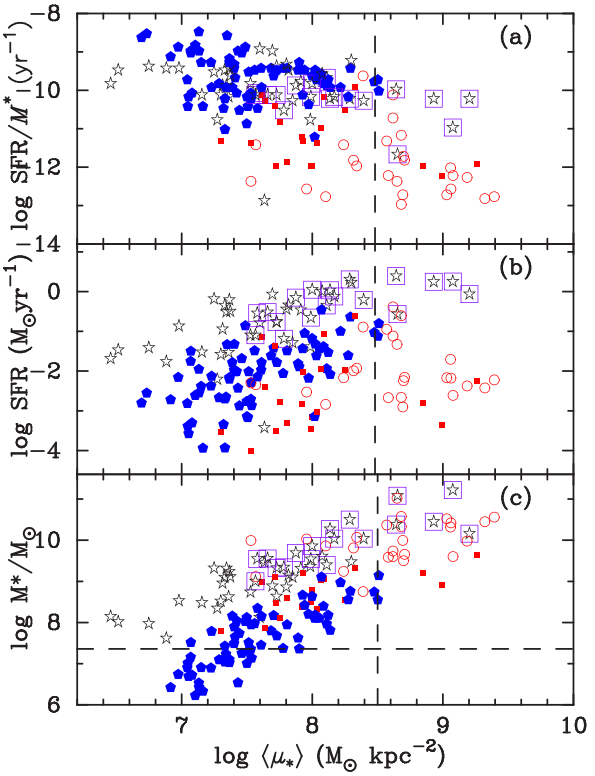

Figure 15. The stellar surface mass density μ_* at $R_{\rm eff}$ as a function of (a) SFR/$M*$, (b) SFR, and (c) $M*$ for the spheroids and spirals in our sample. The vertical dashed line is the characteristic stellar surface mass density of $3 \times 10^8\,{\rm M}_\odot\,{\rm kpc}^{-2}$ reported by Kauffmann et al. (2006).

spiral galaxies is independent of μ_* albeit with large scatter, some of which may be attributed to the weak correlation between $M*$ and SFR (Fig. 5). The sSFR for red spirals is remarkably constrained to $\sim 10^{-10}\,{\rm yr}^{-1}$ despite their $M*$ and μ_* varying by as much as 2 dex. For their relatively more massive sample, Kauffmann et al. (2006) found that sSFR remains constant for all galaxies with log $\mu_* < 8.5\,{\rm M}_\odot\,{\rm kpc}^{-2}$, unlike our sample where low-mass ellipticals and passively evolving lenticulars even below the critical μ_* have lower sSFR than their star-forming counterparts.

We can conclude two things from Fig. 15, first the criticality of the μ_* threshold below which the mean sSFR of galaxies of a given mass and stellar surface density does not depend upon either mass or surface density (Kauffmann et al. 2006) is invalid for our sample with a lower average stellar mass than the sample of Kauffmann et al. Secondly, the BSphs follow a linear relation similar to spirals in the μ_*–$M*$ space, but with a different normalization factor. This analysis therefore shows that for our sample, $M*$ is a function of surface density irrespective of galaxy morphology, unlike the SFR and sSFR for which the trends vary with galaxy morphology.

7 SUMMARY

In this paper, we examine the likelihood of BSph galaxies as progenitors of spiral or elliptical galaxies. In order to do so, we make use of the data products derived from the panchromatic imaging and optical spectra of the GAMA galaxies. This paper presents our complete sample of 432 galaxies (also used in Paper I) spanning the redshift range $0.002 < z < 0.02$, and devoid of very high density environments.

We find that even though BSphs are structurally very similar to ellipticals, the distribution of their luminosity-weighted age, Z, $M_{\rm dust}$,

and sSFR is more like the star-forming spirals than the passively evolving spheroids (ellipticals or lenticulars). BSphs also follow the same SFR–$M_{\rm HI}$ and $M_{\rm HI}$–$M*$ scaling relation as the spirals. We further showed that at any given $M*$, BSphs are more compact than spirals and on average have higher stellar surface mass density at $R_{\rm eff}$ than spiral galaxies, implying that on average their star formation efficiency is lower than spiral galaxies.

The automated clustering algorithm k-means applied to the multidimensional parameter space mapped by age, Z, and $M*$ decomposes the spheroids and spiral galaxies into two 'clusters'. The larger of these comprises 92 per cent of the BSphs but is heavily contaminated (24 per cent) by other types of galaxies having low age, Z, and $M*$. Adding in the $M_{\rm dust}$ to the multidimensional space yields a preference for three clusters, of which the one containing low age, Z, $M_{\rm dust}$, and $M*$ and high sSFR galaxies comprises 85 per cent of the BSphs but is less contaminated (16 per cent) by other galaxy types.

The gas supply for star formation in a galaxy is regulated by the infall of new material on to the parent dark matter halo as it grows. In massive haloes at later times, the time required by the gas to fall and cool becomes much larger than the dynamical time and therefore halts the supply of cold gas for the galaxy. For ΛCDM cosmology, it has been shown that the transition between infall-regulated and cooling flow regime occurs at a halo mass of around 10^{12} $M_{\odot}$ (Birnboim & Dekel 2003; Kereš et al. 2005).

Most of the galaxies in our sample, particularly all the low-mass galaxies, must have infall-regulated supply of gas. Their future is therefore likely to depend on environment: BSphs in the low-density region can accrete more cold gas, therefore developing an intermediate- or large-scale disc, while those in the high-density environment are prone to more lumpy accretion building an elliptical galaxy. A bit of both the processes is likely to result in a low-mass lenticular. It is possible that this is an ongoing process at all redshifts but because these galaxies have low mass, we are only able to observe them locally.

To conclude, our data suggest that although BSph galaxies are structurally similar to ellipticals and have physical and star formation properties like spirals, statistically they are distinguishable from either of them in the multidimensional parameter space mapped by age, Z, $M_{\rm dust}$, and sSFR. Therefore, based on our analysis, we conclude that some BSphs may evolve into disc galaxies in the future, while others in the low-density environments may evolve into small red ellipticals. But their currently observable properties statistically distinguish them from spirals as well as ellipticals.

ACKNOWLEDGEMENTS

GAMA is a joint European-Australasian project based around a spectroscopic campaign using the Anglo-Australian Telescope. The GAMA input catalogue is based on data taken from the SDSS and the UKIRT Infrared Deep Sky Survey. Complementary imaging of the GAMA regions is being obtained by a number of independent survey programmes including *GALEX*, MIS, VST KiDS, VISTA VIKING, *WISE*, Herschel-ATLAS, GMRT, and ASKAP providing UV to radio coverage. GAMA is funded by the STFC (UK), the ARC (Australia), the AAO, and the participating institutions. The GAMA website is http://www.gama-survey.org/. We are grateful to the reviewer for the suggestions and comments which helped improve this manuscript.

SM is funded by the INSPIRE Faculty award (DST/INSPIRE/04/2015/002311), Department of Science and Technology (DST), Government of India.

REFERENCES

Birnboim Y., Dekel A., 2003, MNRAS, 345, 349
Cameron E., Driver S. P., Graham A. W., Liske J., 2009, ApJ, 699, 105
Charrad M., Ghazzali N., Boiteau V., Niknafs A., 2012, NbClust Package: Finding the Relevant Number of Clusters in a Dataset, UseR! 2012. Available at: http://cran.r-project.org/web/packages/NbClust/index.html
da Cunha E., Charlot S., Elbaz D., 2008, MNRAS, 388, 1595
Driver S. P. et al., 2006, MNRAS, 368, 414
Driver S. P. et al., 2011, MNRAS, 413, 971
Driver S. P. et al., 2016, MNRAS, 455, 3911
George K., 2017, A&A, 598, A45
Giovanelli R. et al., 2005, AJ, 130, 2598
Gordon Y. A. et al., 2017, MNRAS, 465, 2671
Graham A. W., Dullo B. T., Savorgnan G. A. D., 2015, ApJ, 804, 32
Graham A. W., Ciambur B. C., Savorgnan G. A. D., 2016, ApJ, 831, 132
Graham A. W., Janz J., Penny S. J., Chilingarian I. V., Ciambur B. C., Forbes D. A., Davies R. L., 2017, ApJ, 840, 68
Gunawardhana M. L. P. et al., 2013, MNRAS, 433, 2764
Haynes M. P. et al., 2011, AJ, 142, 170
Hopkins A. M. et al., 2003, ApJ, 599, 971
Hopkins A. M. et al., 2013, MNRAS, 430, 2047
Janowiecki S., Catinella B., Cortese L., Saintonge A., Brown T., Wang J., 2017, MNRAS, 466, 4795
Kannappan S. J., 2004, ApJ, 611, L89
Kannappan S. J., Wei L. H., 2008, in Minchin R., Momjian E., eds, AIP Conf. Ser. Vol. 1035. The Evolution of Galaxies Through the Neutral Hydrogen Window, Am. Inst. Phys., New York, p. 163
Kannappan S. J., Guie J. M., Baker A. J., 2009, AJ, 138, 579
Kauffmann G., Heckman T. M., De Lucia G., Brinchmann J., Charlot S., Tremonti C., White S. D. M., Brinkmann J., 2006, MNRAS, 367, 1394
Kaviraj S., 2010, MNRAS, 408, 170
Kelvin L. S. et al., 2012, MNRAS, 421, 1007
Kennicutt R. C., Jr, 1998, ARA&A, 36, 189
Kereš D., Katz N., Weinberg D. H., Davé R., 2005, MNRAS, 363, 2
Kim T. et al., 2012, ApJ, 753, 43
Liske J., Lemon D. J., Driver S. P., Cross N. J. G., Couch W. J., 2003, MNRAS, 344, 307
Liske J. et al., 2015, MNRAS, 452, 2087
Lopes P. A. A., Rembold S. B., Ribeiro A. L. B., Nascimento R. S., Vajgel B., 2016, MNRAS, 461, 2559
Loveday J. et al., 2012, MNRAS, 420, 1239
Macqueen J., 1967, in Cam L. M. L., Neyman J., eds, Proc. 5th Berkeley Symp. Math. Stat. Probab. Vol. 1, Statistics. Univ. of California Press, Oakland, p. 281
Mahajan S. et al., 2015, MNRAS, 446, 2967 (Paper I)
Moffett A. J. et al., 2016, MNRAS, 462, 4336
Noeske K. G., Koo D. C., Phillips A. C., Willmer C. N. A., Melbourne J., Gil de Paz A., Papaderos P., 2006, ApJ, 640, L143
Robotham A. et al., 2010, Publ. Astron. Soc. Aust., 27, 76
Schawinski K. et al., 2009, MNRAS, 396, 818
Tonry J. L., Blakeslee J. P., Ajhar E. A., Dressler A., 2000, ApJ, 530, 625
Wright A. H. et al., 2016, MNRAS, 460, 765

SUPPORTING INFORMATION

Supplementary data are available at *MNRAS* online.

data-table-paper.txt

Please note: Oxford University Press is not responsible for the content or functionality of any supporting materials supplied by the authors. Any queries (other than missing material) should be directed to the corresponding author for the article.

This paper has been typeset from a TEX/LATEX file prepared by the author.